Ultrasound Promoted Synthesis and Properties of Chitosan Nanocomposites Containing Carbon Nanotubes and Silver Nanoparticles

Saira Bibi[a,c], Arifa Jamil[b], Tariq Yasin[b], Muhammad Aftab Rafiq[b], Mohsan Nawaz[a], Gareth J. Price[c] *

a. Department of Chemistry, Hazara University, Mansehra, Pakistan.

b. Department of Metallurgy and Materials Engineering, Pakistan Institute of Engineering and Applied Sciences, Islamabad, Pakistan

c. Department of Chemistry, University of Bath, Claverton Down, Bath, BA2 7AY, UK

* Author for correspondence: g.j.price@bath.ac.uk

Abstract

A rapid and facile method to prepare functional chitosan nanocomposite films incorporating silver nanoparticles (AgNPs) has been developed using ultrasound assisted in-situ synthesis, dispersion and crosslinking. Addition of AgNPs and CNTs increased the mechanical strength and extensibility of polymeric chitosan nanocomposites. The films were characterized by transmission electron microscopy (TEM), scanning electron microscopy (SEM), and infrared spectroscopy (IR). TEM showed that ultrasound produced more homogeneous dispersion of AgNPs and nanotubes as a result of breakage of CNTs bundles. Dielectric spectroscopy revealed that the real part of dielectric constant is found to increase with increase in temperature and frequency for both Chi/Ag and Chi/CNTs/Ag nanocomposite films. The conductivity of Chi/CNTs/Ag nanocomposite films was lower than when the CNTs were omitted.

Graphical abstract

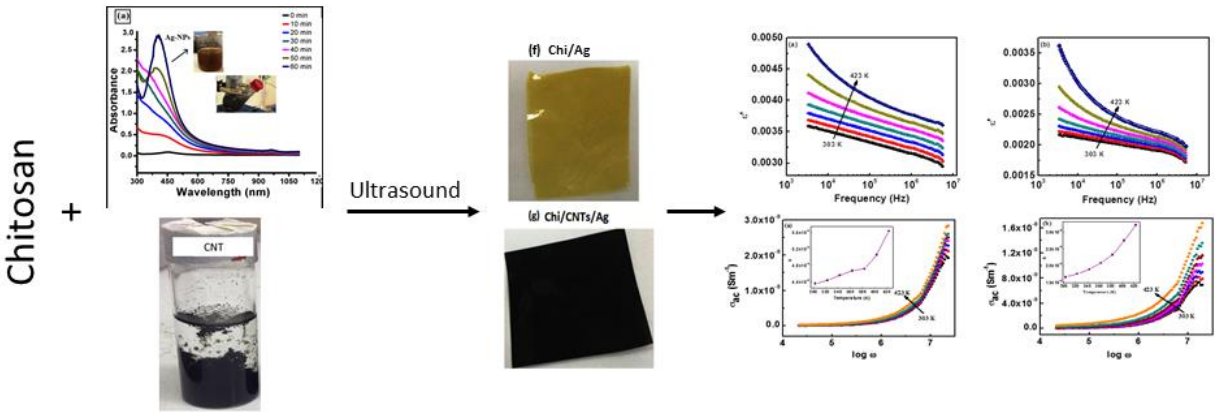

Highlights

- Nanocomposites containing AgNPs and CNTs in chitosan have been prepared
- Use of ultrasound promoted the effective formation and dispersion into the matrix
- Nanocomposite films showed enhanced tensile properties over native chitosan
- Composite properties such as conductivity, impedance and dielectric loss are discussed

Keywords

Ultrasound; chitosan, carbon nanotubes; silver nanoparticles, nanocomposite

1. Introduction

Silver nanoparticles (AgNPs) are gaining enormous attention due to their range of size- and shape-dependent electrical, optical and magnetic properties [1, 2] as well as their potent antibacterial and antifungal activities [3, 4]. AgNPs have been incorporated into polymers to form biosensors, composite materials and fibres, catalysts, cryogenic super conducting materials, cosmetic products and electronic components. They are also being used in clothing, paints, coatings, cosmetics, and electronics, as well as in the food industry [5 - 8]. Several methods have been employed to synthesize AgNPs, including chemical, photochemical or electrochemical reactions or laser ablation [9-11]. The most widely used is the reduction of silver salts by, for example, sodium borohydride or sodium citrate. The use of ultrasound to enhance the synthesis has also been shown to be beneficial [12, 13] and to allow some control over the size and shape of the NPs.

Conducting the synthesis of metal, oxide and chalcogenide nanoparticles using high intensity ultrasound has been widely examined and sonochemistry has developed into a powerful tool in the preparation of nanostructured materials [14, 15] some of which are unavailable by conventional methods [16 - 18]. The primary physical phenomena associated with ultrasound promoted synthesis are due to the generation of acoustic cavitation [19], the growth and explosive collapse of micron sized bubbles in a liquid. Acoustic cavitation can create extreme conditions inside the collapsing bubbles, for example hot spots of ~4500 K, pressures up to~1000 bar and heating and cooling rates of ~10^{10} K s^{-1}, allowing access to a variety of unusual nanostructured materials including a wide range of nanocomposites [14].

The need to produce materials with improved properties has led to the development of a huge range of polymer composites. The latter rely on the incorporation of fillers and modifiers to produce highly functional materials [20]. Among the applications of ultrasound in this area has been the modification of filler surfaces [21] to ensure their efficient dispersal into polymer matrices [22].

This work presents a novel method for the synthesis and effective dispersion of AgNPs and carbon nanotubes (CNTs) in a chitosan matrix. CNTs have been widely used as reinforcing fillers to increase the mechanical strength and elastic moduli of nanocomposite materials [23 - 25]. Our work [26] has recently demonstrated that ultrasound can be used with very dilute acids to overcome the strong van der Waals interactions between CNTs as well as to modify the surface structure and properties so that they can be readily distributed in a chitosan matrix. Chitosan is a naturally occurring biodegradable, cationic polymer. It has been investigated extensively over last decades for use in, amongst others, water treatment, artificial skin and biosensors [27]. Despite its many advantages, chitosan alone has poor mechanical and electrical properties which restrict its use for many applications. The most effective approach to improving these properties is to form a nanocomposite by incorporating components such as clays, metal nanoparticles or nanotubes [28]. Examples incorporating silver have displayed useful properties as heterogeneous catalysts [29] and antibacterial materials [30].

We focus here on, to our knowledge, a novel approach using high power ultrasound for the synthesis of AgNPs and their homogeneous dispersion with CNTs into a chitosan matrix to produce a functional polymer membrane with high mechanical integrity. The effects of including AgNPs and CNTs to form polymeric nanocomposites on the dielectric, morphological, structural and mechanical properties and the implications for their potential uses are reported.

2. Experimental Section

2.1. Materials and Methods

Silver nitrate, chitosan (Chi, C3646, 75% deacetylated), poly(vinyl alcohol) (PVA, Mw: 146,000-186,000), poly(vinyl pyrrolidone) (PVP, average Mw: 40,000), tetraethylorthosilicate, (TEOS), vinyl triethoxysilane (VTES), potassium persulfate, acetic acid, sodium hydroxide, hydrochloric acid and ethanol were obtained from Sigma-Aldrich (UK) and used without further purification. Multi-walled carbon nanotubes, (CNTs), diameter 9.5 nm, and average length 1.5 μm were purchased from Korea (NANOCYL NC700) and were treated with gamma radiation at Pakistan Radiation Services using a ^{60}Co gamma irradiator (Model JS-7900, IR-148, ATCOP) in air at a dose rate of 1.02 kGy h^{-1} to give a total absorbed dose of 200 kGy.

2.2. Synthesis of AgNPs and Chi nanocomposites

Colloidal AgNPs were synthesized from silver nitrate with ultrasonic irradiation by modifying a previously published procedure [9]. Briefly, 100 cm^3 of 0.1 mM aqueous NaOH was sonicated for 1h while adding dropwise 7.2 cm^3 of 5.88 mM aqueous $AgNO_3$ under a nitrogen atmosphere. Sonication was carried out with an ultrasonic horn (Sonic Processor L500-20, Sonic System, 20 kHz), immersed directly into the reaction solution operating at an intensity (measured calorimetrically [31]) of 12 W cm^{-2}. A solution of 0.5g PVP in 5 cm^3 water was added to avoid agglomeration. UV–Visible spectra were recorded every 10 min to monitor the formation of silver nanoparticles (Ag-NPs).

Chi/AgNPs nanocomposite films were also prepared using a modification of a previously reported procedure [32]. Chitosan (1.8 g) was dissolved in 100 cm^3 of 2% acetic acid and 50 cm^3

of the AgNPs suspensions was dispersed in solution by sonication (as above, 12 W cm^{-2}). PVA and PVP (10 mg each) were separately dissolved in 10 cm^3 water and the solutions were mixed with VTES (15.5 µL) and potassium persulfate (0.0125 mg). This mixture was heated to 70 °C for 1 h before adding to the chitosan solution containing TEOS (15.5 µL). Sonication was then carried on at 45°C using a 20 kHz horn at 12 W cm^{-2} for 1 h. The mixture was poured into plastic dishes to dry to form films at room temperature. The same procedure was used for chitosan/CNTs/AgNP synthesis where 1.25 mg of CNTs was dispersed in the PVP solution.

2.3 Characterization

2.3.1. Spectroscopy and Electron Microscopy

UV-visible spectra were recorded using an Agilent-8453 spectrophotometer with distilled water as reference. FT-IR spectra were recorded between 4000 - 500 cm^{-1} using a Perkin Elmer Spectrum 100 spectrometer (16 scans at a resolution of 4.0 cm^{-1}). The AgNPs and the quality of their dispersion with CNTs into the polymer matrix was investigated by transmission electron microscope (TEM) using a JEOL JEM 1200 EXII instrument operated at an accelerating voltage of 120.0 kV. The surface morphology of the nanocomposites was observed by using JEOL SEM-6480LV scanning electron microscope (SEM) operating at 120.0 kV. Samples were prepared by swelling in distilled water and freeze-drying using a Bench-Top Pro Freeze-Dryer. The samples were held on carbon tape and vacuum dried before coating with gold using an Edwards Sputter Coater-S150B. For energy-dispersive spectrometry (EDX) analysis, samples were not coated with gold.

2.3.2. Mechanical and dielectric properties

The mechanical properties of the nanocomposites were measured using an Instron model 3369 material tester. The samples were cut into dumbbell shape with dimensions 30.25 mm × 0.06 mm × 6.6 mm. A 100 N load cell was used with an extension rate of 2 mm min^{-1}. The dielectric properties of Chi/Ag and Chi/CNTs/Ag films were measured with an Agilent 4294A impedance analyzer over a frequency range of 3 kHz to 10 MHz and a temperature range of 303 K to 423 K. The specimen used for measurements had dimensions of 80 mm × 80 mm × 3 mm.

3. Results and discussion

The UV-Vis spectra recorded during the AgNPs synthesis are shown in Fig. 1(a). The growth of the peak corresponding to the surface plasmon resonance (SPR) of nanoparticulate silver was observed in the wavelength range 410-420 nm during the 60 min of sonication. During the reaction, the solution changed from clear, through yellow to a deep brown color. These changes in color and absorption wavelength indicate a modest growth in average particle size of the AgNPs [33]. He e*t al.* reported [12] similar results over the course of 14 h sonication, a much longer reaction time than involved here. The λ_{max} value suggests a final mean particle size of ~ 20 nm. This is supported by our TEM observations where Fig 1(b) shows that the AgNPs are spherical in shape and mostly < 20 nm in diameter although there are a few larger particles.

Figure 1(c, d) show that the ultrasound promoted dispersion of the AgNPs and CNTs into the chitosan matrix is homogeneous; the nanoparticles are well separated from each other. Murugadoss *et al.* suggested that the amine and hydroxyl groups present in chitosan support the nucleation as well as the stabilization of AgNPs [29] by preventing agglomeration and cluster formation. However, in this work nucleation and growth is complete before adding the chitosan. The TEM images also demonstrate that the AgNPs have attached onto CNTs. In this study,

gamma irradiated CNTs were used. Related work [26] has shown that gamma treatment in air partially anneals the CNTs, reducing the number of defect sites and also induces surface oxidation which may facilitate interaction with the AgNPs. Moreover, the CNTs are segregated in the form of separate, untangled tubes, due to the physical effects of sonication during mixing. The absorption spectra and the photographs of the nanocomposite are presented in Figure 1(e-g). The λ_{max} value of the silver absorption band was shifted slightly to longer wavelength after the addition of chitosan into Ag-CNTs dispersion, suggesting a slightly larger average particle size. Interestingly the AgNPs peak after addition of chitosan was somewhat broader than in solution (Fig. 1(a)) suggesting that the size distribution of the nanoparticles may have been broadened.

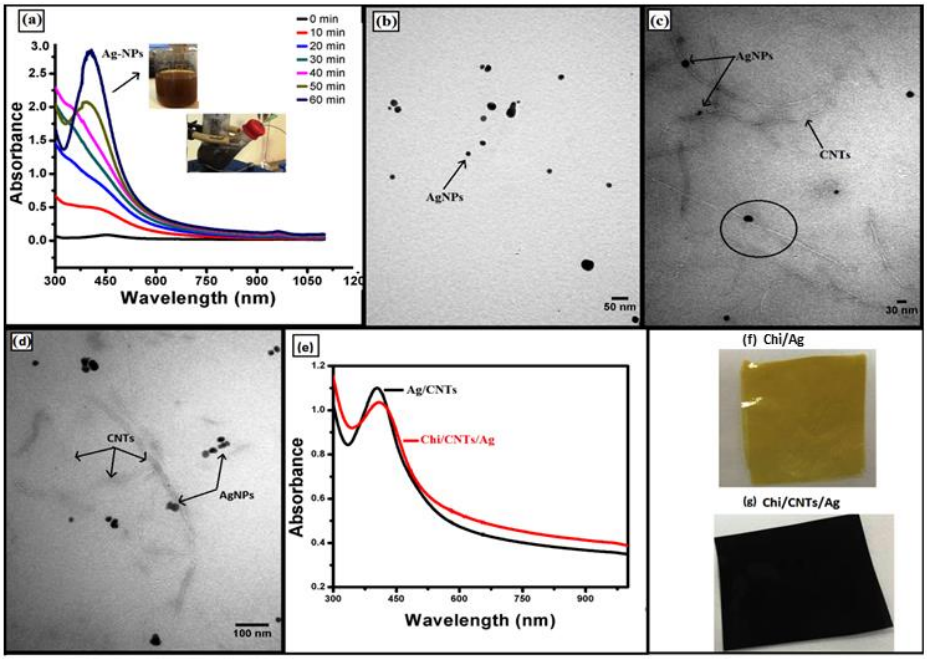

Figure 1. Characterisation of AgNPs and nanocomposites. (a) UV-Vis absorption spectra of AgNPs during synthesis; (b) TEM images of AgNPs synthesized under ultrasound for 1h; (c, d) TEM images of Chi/CNTs/AgNPs; (e), UV-Vis absorption spectra of nanocomposites; (f, g) photographs of cast films.

The SEM micrographs and EDX results for the nanocomposite films are shown in Figure 2. They show the porous nature of the nanocomposite. EDX results confirmed the presence of silver particles in the chitosan matrices. The micrographs suggest that incorporating the CNTs into the film changed the morphology, making them more compact and less porous as has been noted previously. In both cases, the fillers were homogeneously dispersed in the chitosan matrix within the scale of microscopic observation.

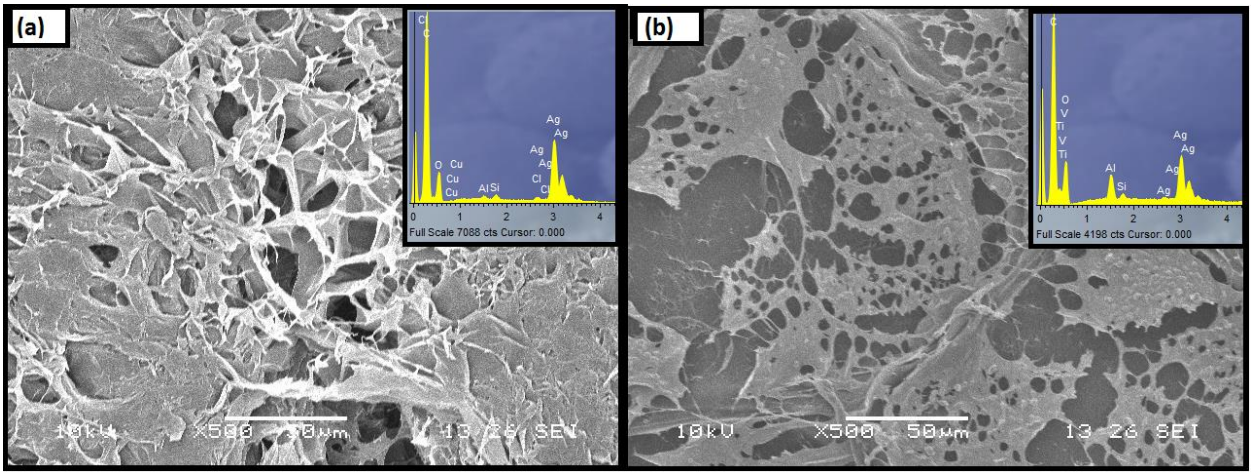

Figure 2. SEM micrographs and EDX spectra (insets) of nanocomposite films. (a) Chi/Ag; (b) Chi/CNTs/Ag

The FTIR spectra of Chi, Chi/AgNP and Chi/CNTs/AgNP films are shown in Figure 3. The Chi spectrum shows absorption peaks at 1652 cm^{-1}, 1542 cm^{-1} and 1325 cm^{-1} corresponding to amide I, amide II and amide III stretches. In the Chi/Ag nanocomposite, the peaks are rather broader around 2850 cm^{-1} due to the increased C-H broad stretching vibrations of the small amounts of PVA and PVP crosslinked in the polymer matrix along with the Chi. The characteristic functional group peaks are shifted after addition of AgNPs in both nanocomposite films indicating that these groups interact with silver or carbon. The peak intensity around 1640 - 1650 cm^{-1} of chitosan increased after adding AgNPs. Vimala *et al*. suggested that the shift was

due to the formation of coordination bonds between metals with the oxygen and nitrogen atoms of chitosan [30]. In this work, the CNTs are partially oxidized by gamma irradiation and so also have the ability to interact with AgNPs and chitosan. The results corroborate those from the TEM above suggesting the attachment of AgNPs to the CNTs.

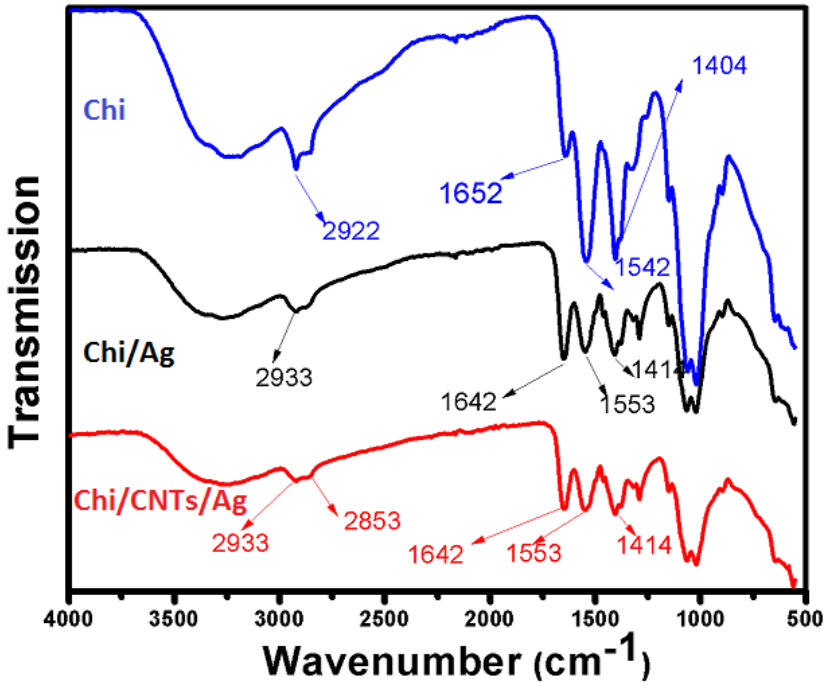

Figure 3. FTIR spectra of chitosan and AgNP-containing nanocomposites

The mechanical properties of a material are crucial in determining its suitability for a particular end use. As shown in Figure 4 and Table 1, incorporation of the AgNPs strengthens the unfilled chitosan film, doubling the tensile strength, toughness and the stress at which the elastic limit was reached although without significantly changing the ultimate strain at break. These improvements result from the interaction between chitosan and the Ag-NPs referred to above which form further physical crosslinks which hold together the polymer matrix. Further, more modest, increases in the tensile properties were observed and the elongation at break extended when CNTs were included in the composite. It should be noted that the exact values

measured depend on the sample history and degree of hydration etc. so the trends here will be valid although further increases could be expected from optimizing the crosslinking density and other properties of the matrix. Similar results were noted when gold nanoparticles were introduced into a chitosan matrix although in that case there was a greater enhancement in tensile strength [34].

Table 1. Mechanical properties of nanocomposite films

Sample	Tensile Strength / MPa	Elongation at break / %	Toughness / J m^{-3}
Chi	4.13	293	6.96
Chi/Ag	8.11	309	13.83
Chi/CNTs/Ag	9.52	345	15.67

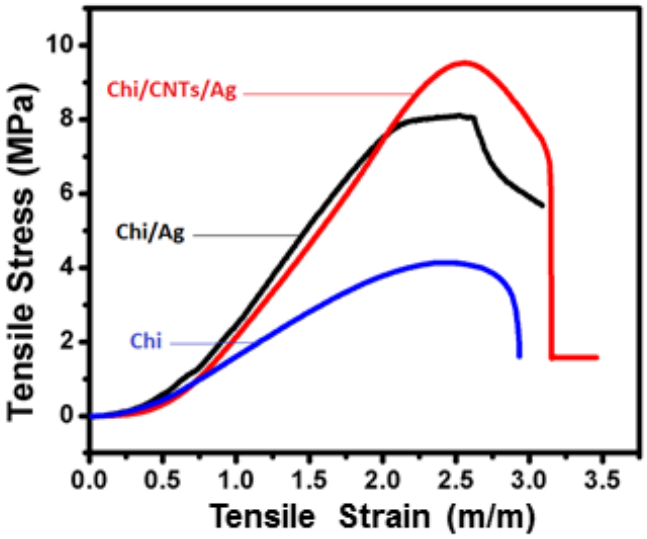

Figure 4. Typical stress-strain curves for nanocomposite films.

Further information on the properties of the nanocomposite films was determined by using impedance spectroscopy to measure the real and imaginary parts of the electrical impedance, Z^*, and dielectric permittivity, ε^*, as a function of the frequency, f, of an applied electric field. These parameters are related to each other by:

$$Z^* = Z' - jZ'' \quad (1)$$

and

$$\varepsilon^* = \varepsilon' - j\varepsilon'' = 1/j\omega C_0 Z^* \quad (2)$$

where Z' and ε' are the real parts and Z'' and ε'' are the imaginary components of the impedance and dielectric permittivity respectively. C_0 is a constant related to the permittivity of free space, ω is the angular frequency ($2\pi f$) and $j = \sqrt{-1}$ [35].

Figure 5 shows the frequency dependence of Z' and Z'' between 303 K to 423 K for the two chitosan nanocomposites. Both Z' and Z'' are higher for the films which contain CNTs since the CNTs make the film more polarizable. Both properties decrease with rising frequency up to ~ 60 kHz for Z' and for Z'' up to ~ 40 kHz above which the values remain very low and constant. The merging of Z' and Z'' indicates space charge liberation at higher frequencies [36]. The fall of Z' and Z'' with increasing frequency for both films is associated with an increase in conduction [37] as thermal activation of dipoles becomes more important [38].

The real component of the ac conductivity, σ_{ac}, can be obtained [36] from:

$$\sigma_{ac} = \left(\frac{Z'}{Z'^2 + Z''^2}\right)\frac{d}{A} = \sigma_1(T) + \sigma_2(\omega, T) \quad (3)$$

where A is the cross-sectional area and d the thickness of a specimen. The dc conductivity, $\sigma_1(T)$, dominates at low frequencies while the final term $\sigma_2(\omega, T)$ captures the temperature and frequency dependence and can be expressed as:

$$\sigma_2(\omega, T) = B(T)\,\omega^s \quad (4)$$

The parameter B has units of electrical conductivity and s is a dimensionless exponent. The variation of σ_{ac} with frequency for the Chi/Ag and Chi/CNTs/Ag films is shown in Figure 6. At low frequencies, the conductivities are low and do not vary much with frequency. This is because the levels of AgNPs and CNTs are below the reported percolation thresholds [39]. It can be seen that σ_{ac} increases markedly at higher frequencies, above ~1 MHz, due to a greater driving force for

the mobility of charge carriers increasing the liberation of charge carriers from trapping centers [40]. As expected, the conductivities are several orders of magnitude higher than the reported values for pristine chitosan films [39] although those values depend critically on the method and conditions of preparation. As the temperature increases, the conductivity increases for both nanocomposites due to the increase in mobility of charge carriers with temperature [41].

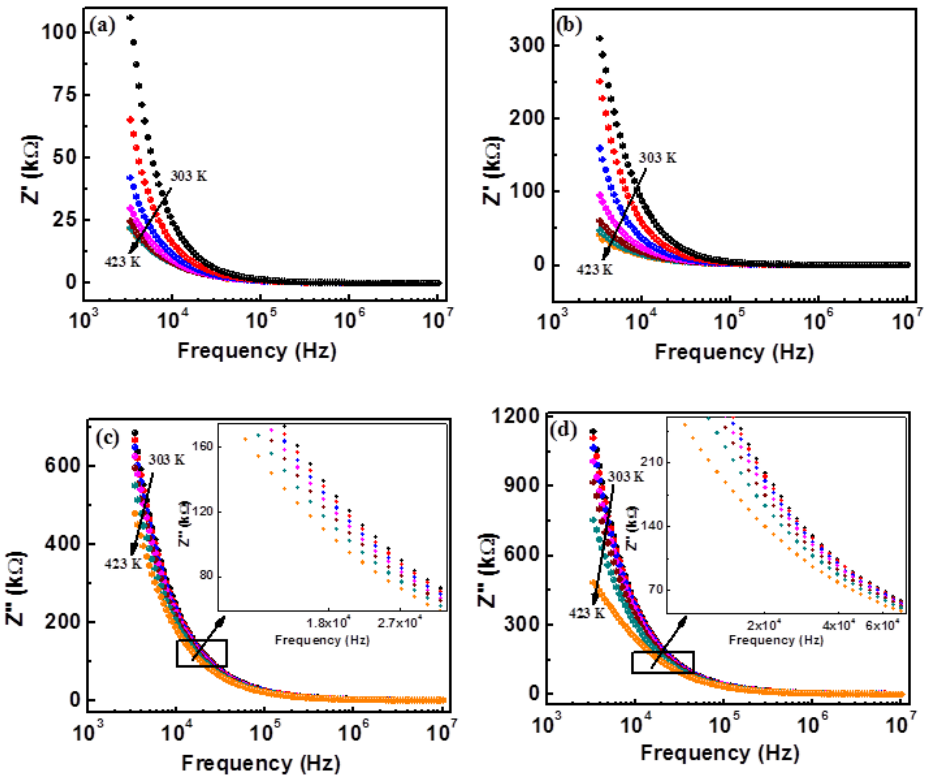

Figure 5. Real (*Z′*) and imaginary (*Z″*) components of impedance as a function of frequency from 303 K to 423 K. (a, c) Chi/Ag; (b, d) Chi/CNTs/Ag

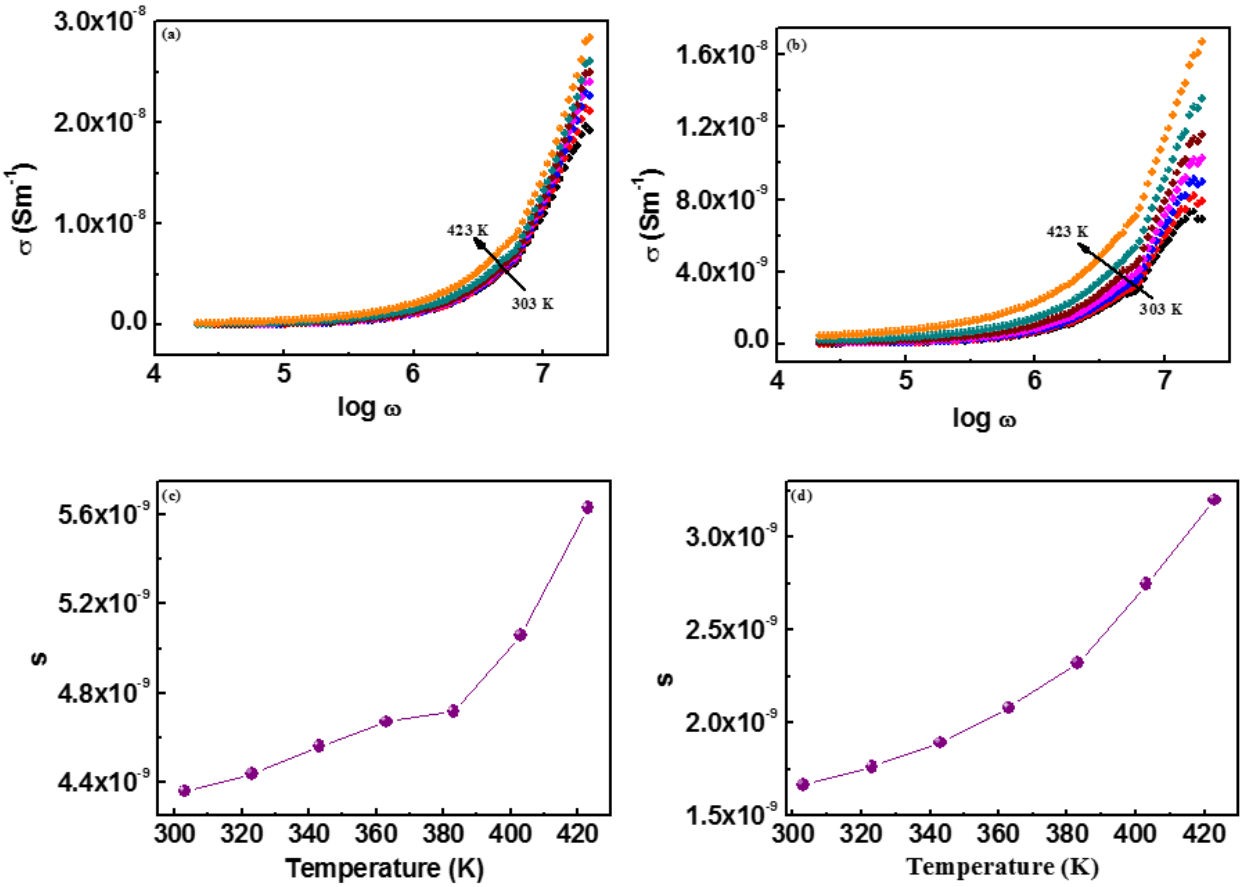

Figure 6. Variation between 303 K to 423 K of ac conductivity with frequency (a, b) and of the frequency exponent from Equation 4 with temperature (c, d). (a, c) Chi/Ag; (b, d) Chi/CNTs/Ag.

The temperature dependence of the frequency exponent, *s*, in Equation (4) yields information on the prevailing charge transport conduction mechanism in a material. It is calculated by nonlinear fitting of Equation (4). If *s* increases with temperature, then the dominant conduction mechanism is by small polarons [42]. If the conduction mechanism is due to overlapping polaron tunneling, *s* first decreases and then increases with rising temperature [43]. Correlated barrier hopping and quantum mechanical tunneling conduction mechanisms are associated with values of *s* that get smaller or are temperature independent. Figure 6(c, d) show that *s* increases with

temperature, suggesting that small polarons are the predominant conduction mechanism in both nanocomposites over the temperature range studied.

The highest measured conductivities occurred at the highest frequency (10 MHz in this work). The values are plotted in Figure 7 to compare the two nanocomposite films. The conductivity, σ_{ac}, is higher for Chi/Ag film than for Chi/CNTs/Ag film at each temperature. This may be due to the interactions between the AgNPs and the CNTs reducing the mobility of the charge carriers in the film [41]. AgNPs on CNTs have been found to be most effective functional conducting fillers, yielding improved electrical applications in epoxy resins due to low contact resistance and high aspect ratios [44]. Again, it should be noted that CNT levels here are below the percolation threshold.

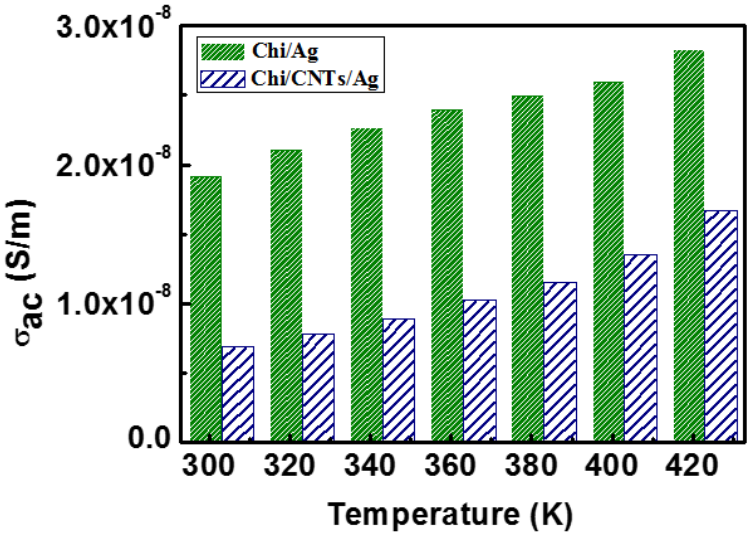

Figure 7. Effect of temperature on conductivity at 10 MHz for Chi nanocomposites.

The frequency and temperature variation of the real part of the dielectric constant, ε', for the nanocomposite films is illustrated in Figure 8. ε' decreases with rising frequency but increases with temperature. No appreciable relaxation peaks were noted over the frequency range measured. The decrease in ε' with frequency is associated with decreasing polarization within the films as the

response time becomes shorter [45]. Different polarization mechanisms such as interfacial, dipolar, atomic, and electronic [46] can operate within a material and each makes a contribution to ε'. At lower frequencies, the time scale is such that each type of polarizations can respond. However, at high frequencies, complete formation of dipoles is not possible so that they do not contribute to the net polarization and hence ε' falls [47]. The low value of ε' at higher frequencies suggests material applications in photonic and electrooptic devices such as waveguides or electrooptic modulators [48]. Conversely, the increase in ε' with rising temperature is due to thermal activation of dipoles [49] and hence higher polarization. A small lowering of ε' was observed on the addition of CNTs in Chi/Ag film at all temperatures.

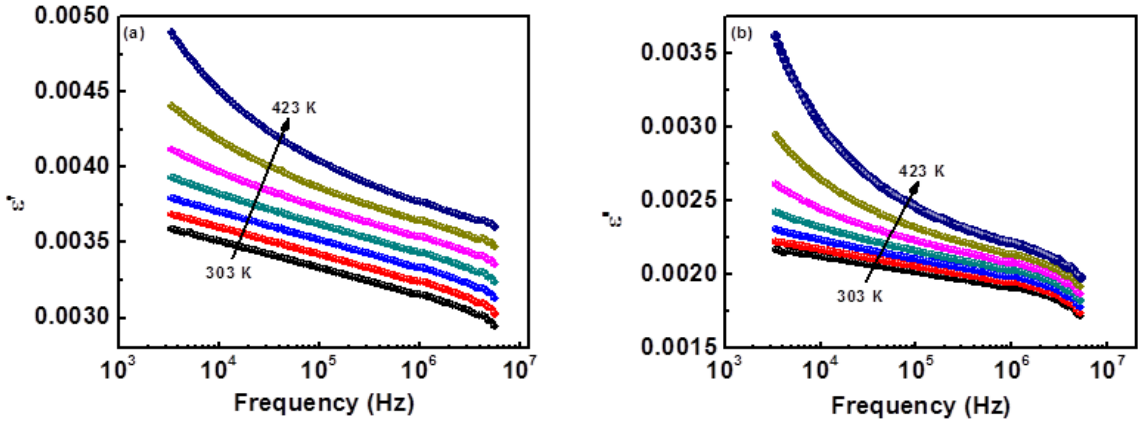

Figure 8. Effect of frequency on ε' from 303 K to 423 K. (a) Chi/Ag; (b) Chi/CNTs/Ag.

The real component of the dielectric constant, ε', represents the energy stored in the medium in an electric field while ε'' accounts for energy losses in the medium. The ratio of these is dielectric loss tangent, tan δ:

$$\tan \delta = \frac{\varepsilon''}{\varepsilon'} \qquad (5)$$

The values for the two nanocomposite films over the frequency range studied are shown in Figure 9. At lower frequencies, there is a large temperature dependence and tan δ takes higher values at higher temperatures. At low temperature, there is no frequency dependence below the MHz range. Chitosan films contain small amounts of H^+, NH_3^+ and acetate ions and the behaviour of tan δ can be explained in terms of ion migration as well as enhanced polarization causing higher losses [50]. Ionic effects are reduced at higher frequencies and hence dielectric losses are lower [51]. Figure 9 also shows an increase in tan δ with temperature. The transitions in the loss spectra in the MHz range suggest that dipolar relaxation is making a contribution to energy dissipation [52, 53]. Addition of elongated CNTs provides further opportunities for interfacial polarization and dipolar interactions which lead to higher loss factors [54, 55].

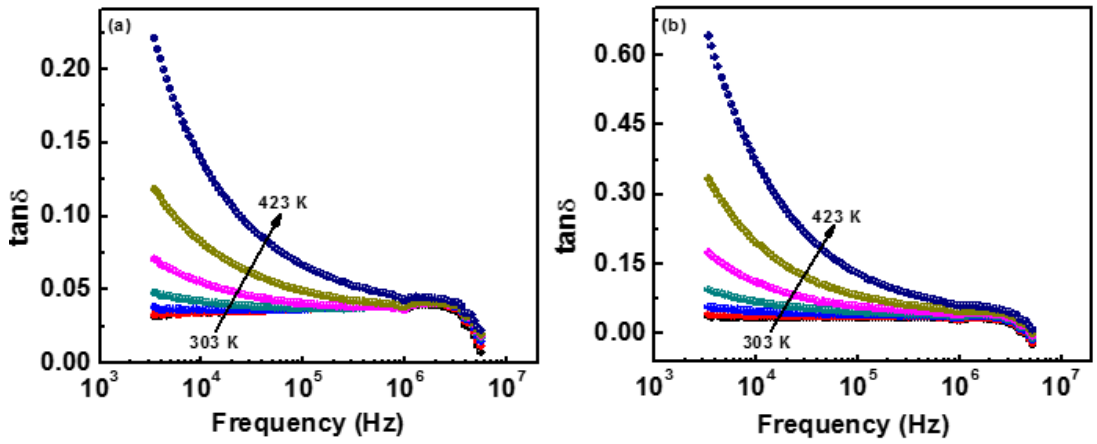

Figure 9. Effect of frequency on tan δ from 303 K to 423 K. (a) Chi/Ag; (b) Chi/CNTs/Ag

4. Conclusion

A new rapid and facile ultrasound-assisted procedure was developed for manufacturing Chitosan nanocomposites with excellent dispersion of CNTs and AgNPs. Data on mechanical properties shows that both fillers have a positive effect on the tensile strength and elongation at break of chitosan. This indirectly indicates better dispersion of the nanotubes and AgNPs in chitosan

under ultrasonic treatment. TEM results also show that ultrasound helps in dispersion of nanotubes as a result of breakage of CNTs bundles. The real part of the dielectric constant was found to increase with increase in temperature and frequency for both Ag/Chi and Ag/Chi/CNTs samples which suggests potential material applications in photonic and electro-optic devices. The dielectric loss factor increased with the addition of elongated CNTs in Ag/Ch film which will limit the usefulness of these nanocomposites in dielectric applications.

Acknowledgements

One of the authors, Saira Bibi, gratefully acknowledges the Higher Education Commission, Pakistan for providing financial funding under IRSIP to visit the University of Bath. We are grateful to Dr Ursula Potter for assistance with the electron microscopy and to Mr Matthew Ball for help with the mechanical property measurements.

References

1. S. Link, M.A. El-Sayed Spectral Properties and Relaxation Dynamics of Surface Plasmon Electronic Oscillations in Gold and Silver Nanodots and Nanorods *J. Phys. Chem. B*, Vol. 1999:103(40):8410–8426
2. K.L. Kelly, E. Coronado, L.L. Zhao, G.C. Schatz The Optical Properties of Metal Nanoparticles: The Influence of Size, Shape, and Dielectric Environment *J. Phys. Chem. B* 2003:107:668 – 677
3. C. Marambio-Jones, E.M. Hoek, A review of the antibacterial effects of silver nanomaterials and potential implications for human health and the environment, *J. Nanoparticle Res.*, 12 (2010) 1531-1551.
4. S. Chernousova, M. Epple Silver as Antibacterial Agent: Ion, Nanoparticle and Metal *Angew.Chem.Int.Ed.*2013:52:1636–1653
5. Z.-J. Jiang, C.-Y. Liu, L.-W. Sun, Catalytic properties of silver nanoparticles supported on silica spheres, *J. Phys. Chem. B,* 109 (2005) 1730-1735
6. D. Chen, X. Qiao, X. Qiu, J. Chen, Synthesis and electrical properties of uniform silver nanoparticles for electronic applications, *J. Mater. Sci.*, 44 (2009) 1076-1081.
7. V.K. Sharma, R.A. Yngard, Y. Lin, Silver nanoparticles: green synthesis and their antimicrobial activities, *Adv. Coll. Interface Sci.*, 145 (2009) 83-96.
8. B. Reidy, A. Haase, A. Luch, K.A. Dawson, I. Lynch, Mechanisms of Silver Nanoparticle Release, Transformation and Toxicity: A Critical Review of Current Knowledge and Recommendations for Future Studies and Applications *Materials* 2013:6(6):2295-2350
9. H. Wang, X. Qiao, J. Chen, S. Ding, Preparation of silver nanoparticles by chemical reduction method, *Coll. Surf. A: Physicochem. Eng. Aspects*, 256 (2005) 111-115.
10. G.R. Nasretdinova, R.R. Fazleeva, R.K. Mukhitova, I.R. Nizameev, M.K. Kadirov, A.Y. Ziganshina, V.V. Yanilkin, Electrochemical synthesis of silver nanoparticles in solution, *Electrochem. Commun.*, 50 (2015) 69-72.
11. M. Wuithschick, B. Paul, R. Bienert, A. Sarfraz, U. Vainio, M. Sztucki, R. Kraehnert, P. Strasser, K. Rademann, F. Emmerling, J. Polte Size-controlled synthesis of colloidal silver nanoparticles based on mechanistic understanding. *Chem. Mater.* 25(23) (2013) 4679-89.
12. C. He, L. Liu, Z. Fang, J. Li, J. Guo, J. Wei, Formation and characterization of silver nanoparticles in aqueous solution via ultrasonic irradiation, *Ultrasonics Sonochem.*, 21 (2014) 542-548.
13. D. Radziuk, D. Shchukin, H. Möhwald Sonochemical Design of Engineered Gold−Silver Nanoparticles *J. Phys. Chem. C*, 112 (2008) 2462–2468
14. K. S. Suslick and G. J. Price, *Ann. Rev. Mater. Sci.*, 29 (1999) 295-326..
15. S. Manickam, M. Ashokkumar (Eds) *Cavitation: A novel Energy-efficient teachnique for the generation of nanomaterials* Pan Stanford Singapore 2014

16. L.-P. Jiang, S. Xu, J.-M. Zhu, J.-R. Zhang, J.-J. Zhu, H.-Y. Chen, Ultrasonic-assisted synthesis of monodisperse single-crystalline silver nanoplates and gold nanorings, *Inorg. Chem.*, 43 (2004) 5877-5883.

17. H. Xu, B.W. Zeiger, K.S. Suslick, Sonochemical synthesis of nanomaterials, *Chem. Soc. Rev.*, 42 (2013) 2555-2567.

18. A. Gedanken, "Using sonochemistry for the fabrication of nanomaterials," *Ultrasonics Sonochem.*, 11 (2004) 47-55.

19. M. Ashokkumar, "The characterization of acoustic cavitation bubbles – An overview," *Ultrasonics Sonochem.*, 18 (2011) 864-872.

20. *Polymer Composites, Vol. 2, Nanocomposites* S. Thomas, K. Joseph, S. K. Malhotra, Koichi Goda, M. S. Sreekala (Eds) Wiley, Chichester ISBN: 978-3-527-32979-3

21. K. Zhang, B.J. Park, F.F. Fang and H.J. Choi Sonochemical Preparation of Polymer Nanocomposites *Molecules* 2009, *14*, 2095-2110

22. J-E. Park, M. Atobe, T. Fuchigami Sonochemical synthesis of conducting polymer–metal nanoparticles nanocomposite *Electrochim. Acta* 51(5), 2005, 849–854

23. T.E. Chang, A. Kisliuk, S.M. Rhodes, W.J. Brittain and A.P. Sokolov Conductivity and mechanical properties of well-dispersed single-wall carbon nanotube/polystyrene composite *Polymer* 2006 47, 7740–7746

24. J.A. Kim, D.G. Seong, T.J. Kang, J.R. Youn Effects of surface modification on rheological and mechanical properties of CNT/epoxy composites *Carbon* 2006, 44, 1898–1905

25. J. B. Marroquin, K.Y. Rhee, S.J. Park Chitosan nanocomposite films: Enhanced electrical conductivity, thermal stability, and mechanical properties *Carbohydrate Polymers*, 92 (2013) 1783-1791

26. S.Bibi, T. Yasin, M. Nawaz, G.J. Price Comparative study of the modification of multi-wall carbon nanotubes by gamma irradiation and sonochemically assisted acid etching techniques. *Mater. Chem. Phys.* 207, 23 – 29 (2018)

27. H. Tamura, T. Furuike, Chitin and Chitosan, *Encyclopedia of Polymeric Nanomaterials*, (2015) 386-389.

28. C. Shan, *et al.*, "Graphene/AuNPs/chitosan nanocomposites film for glucose biosensing," *Biosensors and Bioelectronics*, vol. 25, pp. 1070-1074, 2010.

29. A. Murugadoss, A. Chattopadhyay, A 'green'chitosan–silver nanoparticle composite as a heterogeneous as well as micro-heterogeneous catalyst, *Nanotechnology*, 19 (2007) 015603

30. K. Vimala, Y.M. Mohan, K.S. Sivudu, K. Varaprasad, S. Ravindra, N.N. Reddy, Y. Padma, B. Sreedhar, K. MohanaRaju, Fabrication of porous chitosan films impregnated with silver nanoparticles: a facile approach for superior antibacterial application, *Coll. Surf. B: Biointerfaces*, 76 (2010) 248-258.

31. S. Koda, T. Kimura, T. Kondo, H. Mitome, A standard method to calibrate sonochemical efficiency of an individual reaction system *Ultrasonics Sonochem*., 10 (2003) 149-156

32. S. Bibi, T. Yasin, S. Hassan, M. Riaz and M. Nawaz, Chitosan/CNTs nanocomposite as green carrier material for pesticides controlled release *Mater. Sci. Eng.:C*, 2015, **46**, 359-365.

33. H. Huang, Q. Yuan, X. Yang, Preparation and characterization of metal–chitosan nanocomposites, *Coll. Surf. B: Biointerfaces*, 39 (2004) 31-37.

34. S.Bibi, G.J. Price, T. Yasin, M. NawazEco-friendly synthesis and catalytic application of Chitosan/Gold/ Carbon Nanotube nanocomposite films *RSC Advances* **6**, 60180 – 60186 (2016)

35. E. Barsoukov and J. R. Macdonald, *Impedance spectroscopy: theory, experiment, and applications*: John Wiley & Sons, 2005.

36. M. Ahmad, M. Rafiq, M. Hasan, Transport characteristics and colossal dielectric response of cadmium sulfide nanoparticles, *J. Appl. Phys*., 114 (2013) 133702.

37. A.M.Farea, S. Kumar, K.M. Batoo, A. Yousef, C.G. Lee, A. Muddin., Structure and electrical properties of Co 0.5 Cd x Fe 2.5− x O 4 ferrites, *J. Alloys and Compounds,* **464**, 361-369 (2008)

38. R. Gerhardt, "Impedance and dielectric spectroscopy revisited: distinguishing localized relaxation from long-range conductivity," *J. Phys. Chem. Solids*, 55, 1491-1506, 1994.

39. E. Prokhorov, J.G. Luna-Bárcenas, J.B. González-Campos, I.C. Sanchez *Mol. Cryst. Liq. Cryst*., 2011, 536:1, 24-32

40. E.V.Gopalan, K.A.Malini, S.Sagar, D.S. Kumar, Y.Yoshida, I. A. Al-Omari, M. R. Anantharaman, Mechanism of ac conduction in nanostructured manganese zinc mixed ferrites, *J. Phys. D: Appl. Phys*. 42 (2009) 165005.

41. J.H.Vargas, J.B. G.Campos, J.L.Romero, E. Prokhorov,G.L.Barcenas, J.A.A.Verduzco, J.C.G.Hernandez,Chitosan/MWCNTs-Decorated with Silver Nanoparticle Composites:Dielectric and Antibacterial Characterization, *J. Appl. Polym. Sci*., (2014) 40214

42. T. Meaz, S. Attia, A.A. El Ata, Effect of tetravalent titanium ions substitution on the dielectric properties of Co–Zn ferrites, *J. Magnetism and Magnetic Materials*, 257 (2003) 296-305.

43. A. Ghosh, AC conduction in iron bismuthate glassy semiconductors, *Phys. Rev. B*, 42 (1990) 1388.

44. P.C. Ma, B.Z. Tang, J.-K. Kim, Effect of CNT decoration with silver nanoparticles on electrical conductivity of CNT-polymer composites, *Carbon*, 46 (2008) 1497-1505.

45. A.S. Bhatt, D. Krishna Bhat, M.S. Santosh Electrical and magnetic properties of chitosan-magnetite nanocomposites *Physica B: Condensed Matter* 405(8), 2010, 2078-2082

46. A. ur Rahman, M. Rafiq, S. Karim, K. Maaz, M. Siddique, M. Hasan, Reduced conductivity and enhancement of Debye orientational polarization in lanthanum doped cobalt ferrite nanoparticles, *Physica B: Condensed Matter*, 406 (2011) 4393-4399.

47. A. Jamil, S. Batool, F. Sher, M. Rafiq, Determination of density of states, conduction mechanisms and dielectric properties of nickel disulfide nanoparticles, *AIP Advances*, 6 (2016) 055120.

48. Y. Enami, C.T. Derose, D. Mathine, C. Loychik, C. Greenlee, R.A. Norwood, T.D. Kim, J. Luo, Y. Tian, A.K. Jen, N. Peyghambarian Hybrid polymer/sol–gel waveguide modulations with exceptionally large electro–optic coefficients *Nature Photonics* 1, 180–185 (2007)

49. N. Kanagathara, N. Renganathan, M. Marchewka, N. Sivakumar, K. Gayathri, P. Krishnan, S. Gunasekaran, G. Anbalagan, Growth and characterization of Melaminium bis (trichloroacetate) dihydrate, *Spectrochimica Acta Part A: Molecular and Biomolecular Spectroscopy*, 101 (2013) 112-118.

50. A. Kool, P. Thakur, B. Bagchi, N.A. Hoque, S. Banerjee, S. Das, Sol–gel synthesis of transition-metal ion conjugated alumina-rich mullite nanocomposites with potential mechanical, dielectric and photoluminescence properties, *RSC Advances*, 5 (2015) 104299-104313.

51. A. Tabib, N. Sdiri, H. Elhouichet, M. Férid, Investigations on electrical conductivity and dielectric properties of Na doped ZnO synthesized from sol gel method, *J. Alloys and Compounds*, 622 (2015) 687-694.

52. S.A. Mir, M. Ikram, K. Sultan, Z. Habib, H. Kausar, K. Asokan, Correlative exploration of structural, optical and electric properties of colossal dielectric Ni doped sm orthoferrites. Adv. Mater. Lett., 6 (2015), 1081-1087

53. A. Wypych, I. Bobowska, M. Tracz, A. Opasinska, S. Kadlubowski, A. Krzywania-Kaliszewska, J. Grobelny, P. Wojciechowski, Dielectric properties and characterisation of titanium dioxide obtained by different chemistry methods, *J. Nanomaterials*, 2014 (2014).

54. J.-P. Peng, H. Zhang, L.-C. Tang, Y. Jia, Z. Zhang, Dielectric properties of carbon nanotubes/epoxy composites, *Nanoscience and Nanotechnology*, 13 (2013) 964-969.

55. C. Yang, Y. Lin, C. Nan, Modified carbon nanotube composites with high dielectric constant, low dielectric loss and large energy density, *Carbon*, 47 (2009) 1096-1101.